Modeling molecular magnets with large exchange and on-site anisotropies

Sumit Haldar,[1,*] Rajamani Raghunathan,[2,†] Jean-Pascal Sutter,[3,‡] and S. Ramasesha[1,§]
[1]*Solid State and Structural Chemistry Unit, Indian Institute of Science, Bangalore 560012, India*
[2]*UGC-DAE Consortium for Scientific Research, Indore 452017, India*
[3]*LCC-CNRS, Université de Toulouse, CNRS, Toulouse, France*

(Received 18 June 2018; revised manuscript received 6 November 2018; published 7 December 2018)

Spins in molecular magnets can experience both anisotropic exchange interactions and on-site magnetic anisotropy. In this paper, we study the effect of exchange anisotropy on the molecular magnetic anisotropy both with and without on-site anisotropy. When both the anisotropies are small, we find that the axial anisotropy parameter D_M in the effective spin Hamiltonian is the sum of the individual contributions due to exchange and on-site anisotropies. We find that even for axial anisotropy of about 15%, the low-energy spectrum does not correspond to a single-parent spin manifold but has intruder states arising from other parent spins. In this case, the low-energy spectrum cannot be described by multiplet states arising from a single approximate total spin state. We study the magnetic susceptibility, specific heat as a function of temperature, and magnetization as a function of applied field to characterize the system in this limit. We find that there is synergy between the two anisotropies, particularly for large systems with higher site spins.

DOI: 10.1103/PhysRevB.98.214409

I. INTRODUCTION

Molecular spin clusters such as single-molecule magnets (SMMs) and single-chain magnets (SCMs) have been studied extensively over the last few decades [1–10]. The main bottleneck for application of these systems in technologies appears to be the fast relaxation of the magnetization from the fully magnetized to the nonmagnetized state for the presently known SMMs and SCMs [11,12]. This is due to the low blocking temperature (measured as the temperature at which the relaxation time for magnetization, τ_R, is 100 s), which depends on the energy barrier between two fully and oppositely magnetized states. Hence, research in this field is focused on enhancing the blocking temperature [13,14].

The energy barrier Δ, between two fully and oppositely magnetized states of an anisotropic spin cluster of spin S is given by $\Delta = |D_M|S^2$ for an integer spin cluster and $|D_M|(S^2 - 1/4)$ for a half-integer spin cluster. Therefore, there are two routes to enhancing Δ: (i) by increasing D_M and (ii) by increasing S. Increasing D_M can be achieved by using magnetic building blocks in unusual coordination numbers and geometry. Indeed, this has been demonstrated for hepta coordinated complexes [15–19]. Increasing S can be achieved by using rare earth ions as the building blocks. However, it has been shown by Waldmann [20] that the magnetic anisotropy of a ferromagnetic assembly of spins is smaller than the anisotropy of individual spins, as each spin center with spin s_i only contributes a fraction,

$$\frac{s_i(2s_i - 1)}{S(2S - 1)}, \tag{1}$$

of the site anisotropy to the anisotropy of the SMM or SCM with total spin S. This result assumes that all the individual magnetic ions have nonzero axial anisotropy d_i and zero planar anisotropy e_i, and that all the spin centers have the same magnetic axes. Notwithstanding this nuance, the result is illustrative of the fact that the anisotropy of the clusters is smaller than that of individual ions.

With $3d$ transition-metal complexes, the highest blocking temperature reported is 4.5 K, although the energy barrier Δ is 62 cm^{-1} [21]. This could be due to the large off-diagonal anisotropy terms that lead to quantum tunneling of magnetization. The anisotropy can be enhanced by choosing ions of $4d$, $5d$, or $4f$ metals wherein the relativistic effects are large, leading to large spin-orbit interactions [13,22,23,25]. For example, in the Dy_4 systems, the energy barrier is 692 cm^{-1} [26]. However, large quantum tunneling of magnetization leads to small hysteresis loops. In our previous studies [27], we have shown that large magnetic anisotropy of building blocks leads to significant breaking of the spin symmetry. In this event, associating a parent spin state[1] to define the D_M and E_M parameters of a cluster is not possible due to intrusion of states from different parent spins within the given spin manifold. This has also been shown experimentally by magnetic relaxation studies of Mn_6 nanomagnets [29]. Lippert *et al.* [30] have also shown that increasing the gap between the ground spin state and the excited spin states will slow down the magnetic relaxation, both thermal and quantum

*sumithaldar@iisc.ac.in
†rajamani@csr.res.in
‡jean-pascal.sutter@lcc-toulouse.fr
§Corresponding author: ramasesh@iisc.ac.in

[1]Parent spin is the spin of the state from which the multiplets arise due to anisotropic terms in the Hamiltonian.

tunneling, leading to larger effective barrier. In these cases, the Waldmann conclusion that the contribution of the individual anisotropies decreases with increasing total spin of the cluster, resulting in smaller barriers, is no longer valid. The properties of the system will have to be computed from the eigenstates of the full Hamiltonian.

The origin of single ion anisotropy as well as anisotropic exchange interactions lie in spin-orbit interactions. Indeed, it is difficult to assume isotropic or simple Heisenberg exchange interactions between spin sites that are highly anisotropic. High nuclearity complexes with large anisotropic interactions are known in a few cases, $[Mn_6{}^{\mathrm{III}}\mathrm{Os}^{\mathrm{III}}]^{3+}$ cluster has $J^x = -9\,\mathrm{cm}^{-1}$, $J^y = +17\,\mathrm{cm}^{-1}$ and $J^z = -16.5\,\mathrm{cm}^{-1}$ [24,31,32] and $[Mn^{\mathrm{II}}\mathrm{Mo}^{\mathrm{III}}]$ complex has $J^z = -34\,\mathrm{cm}^{-1}$ and $J^x = J^y = -11\,\mathrm{cm}^{-1}$ [33,34]. In this paper, we employ a generalized ferromagnetic XYZ model for nearest-neighbor spin-spin interactions and on-site anisotropy. Using the full Fock space of the Hamiltonian, we follow the properties such as magnetization, susceptibility, and specific heat of spin chains with ferromagnetic interaction and different site spins. In the next section, we discuss briefly spin Hamiltonians we have studied and present the numerical approach for obtaining the properties of the model. In Sec. III, we present the result of a purely anisotropic exchange model. This will be followed by the results on a model with both exchange and site anisotropies in Sec. IV. We will end the paper with a discussion of all the results.

II. METHODOLOGY

The basic starting Hamiltonian for studying most magnetic materials is the isotropic Heisenberg exchange model given by

$$\hat{\mathcal{H}}_{\mathrm{Heis}} = \sum_{\langle i,j\rangle} J_{ij}\, \hat{\vec{s}}_i \cdot \hat{\vec{s}}_j, \tag{2}$$

where the summation is over nearest neighbors. Our study is confined to ferromagnetic open chains with nearest-neighbor exchange interactions. Hence $J_{ij} = J_{i,i+1} = J < 0$, with all site spins having the same spin of either 1, 3/2, or 2. This model assumes that spin-orbit interactions are weak and hence the exchange constant J associated with the three components of the spin are equal ($J^x_{ij} = J^y_{ij} = J^z_{ij}$). The isotropic model conserves both total M_s and total S, and hence we can choose a spin-adapted basis such as the valence bond (VB) basis to set up the Hamiltonian matrix. The Rumer-Pauling VB basis is nonorthogonal and hence the Hamiltonian matrix is nonsymmetric. While computing eigenstates of a nonsymmetric matrix is reasonably straightforward, computing properties of the eigenstates in the VB basis is nontrivial. However, the VB eigenstates can be transformed to eigenstates in constant M_s basis, and the latter basis being orthonormal is easily amenable to computing properties of the eigenstates [35].

When the spin-orbit interactions are weak, we can include the anisotropy arising from it by adding the site anisotropy term,

$$\hat{\mathcal{H}}_{\mathrm{aniso}} = \sum_i \hat{\vec{s}}_i \cdot \bar{\bar{D}}_i \cdot \hat{\vec{s}}_i, \tag{3}$$

TABLE I. Energy gaps (in units of $|J|$) from the ground state of the low-lying states lying below the lowest state with $M_s = 0$. M_s is conserved and is a good quantum number. The total spin S_{tot} is calculated from the expectation value $\langle \hat{S}^2 \rangle$ of the state. Intruder states are shown in red.

	$N = 5$, XXZ model								
ϵ	$s = 1$			$s = 3/2$			$s = 2$		
	M_s	S_{tot}	Energy	M_s	S_{tot}	Energy	M_s	S_{tot}	Energy
0.10	±5	5.00	0	±7.5	7.50	0	±10	10.00	0
	±4	4.99	0.158	±6.5	7.49	0.237	±9	9.99	0.316
	±3	4.99	0.282	±5.5	7.49	0.442	±8	9.99	0.601
	±2	4.99	0.370	±4.5	7.49	0.612	±7	9.99	0.852
	±1	4.99	0.423	±6.5	6.50	0.706	±9	9.00	0.941
	0	4.99	0.441	±3.5	7.49	0.749	±6	9.99	1.071
				±2.5	7.49	0.852	±8	8.99	1.217
				±5.5	6.49	0.902	±5	9.99	1.256
				±1.5	7.49	0.921	±4	9.99	1.407
				±0.5	7.49	0.955	±7	8.99	1.462
							±3	9.99	1.526
							±2	9.99	1.610
							±1	9.99	1.661
							±6	8.99	1.673
							0	9.99	1.678
0.15	±5	5.00	0	±7.5	7.50	0	±10	10.00	0
	±4	4.99	0.236	±6.5	7.49	0.354	±9	9.99	0.472
	±3	4.99	0.420	±5.5	7.49	0.658	±8	9.99	0.895
	±4	4.00	0.514	±6.5	6.50	0.771	±9	8.99	1.028
	±2	4.98	0.551	±4.5	7.489	0.914	±7	9.991	1.272
	±1	4.98	0.630	±5.5	6.49	1.063	±8	8.99	1.441
	0	4.97	0.656	±3.5	7.48	1.118	±6	9.98	1.598
				±2.5	7.48	1.273	±7	8.99	1.805
				±4.5	6.49	1.305	±5	9.98	1.876
				±1.5	7.48	1.375	±8	8.00	2.050
				±0.5	7.48	1.426	±4	9.98	2.104
							±6	8.98	2.120
							±3	9.98	2.282
							±5	8.97	2.386
							±7	8.00	2.399
							±2	9.98	2.408
							±1	9.98	2.484
							0	9.98	2.510

where D_i is the anisotropy matrix. If the anisotropy matrix D_i is identical for all spins, we can rotate the spin axis to coincide with the direction of the eigenvectors of D. In this case, the Hamiltonian can be written as

$$\hat{\mathcal{H}}_{\mathrm{aniso}} = \sum_i \left[d_z \hat{s}^2_{i,z} + d_x \hat{s}^2_{i,x} + d_y \hat{s}^2_{i,y} \right], \tag{4}$$

(d_x, d_y, and d_z are local ion anisotropies) and treating it as a perturbation. Usually, it is sufficient to deal with just the z component of the site diagonal anisotropy and set $d_x = d_y = 0$. If the local anisotropy axis is not aligned with the global spin axis, then it will generate other components of the anisotropy parameter when all of them are referred to the global axis. In our study, we have confined ourselves only to uniaxial site diagonal anisotropy, i.e., $d = d_z < 0$ and

TABLE II. Molecular anisotropy parameter $D_M(S)$ for different multiplets arising from total spins 10, 9, and 8 in a $s = 2$ spin chain of five sites for different ϵ and d/J values. $D_M(S)$ values are computed by fitting the energy gaps to $D_M(S)S_z^2$ using a least-squares algorithm.

	$N = 5, s = 2$					
Approximate	$d/J = 0, \epsilon = 0.1$		$d/J = 0.1, \epsilon = 0.1$		$d/J = 0, \epsilon = 0.15$	
total spin	E_0	$D_M(S)$	E_0	$D_M(S)$	E_0	$D_M(S)$
10	0.0	−0.0168	0.0	−0.0321	0.0	−0.0251
9	0.58	−0.0162	0.38	−0.0289	0.49	−0.0244
8	1.20	−0.0155	0.85	−0.0255	1.02	−0.0230

$d_x = d_y = 0$. For weak on-site anisotropy ($\frac{d}{J} \ll 1$), we can obtain the splitting of the multiplets of a given total spin state perturbatively by determining the molecular anisotropy parameters D_M and E_M given by the eigenstates of the Hamiltonian in a given spin state S [36],

$$\hat{\mathcal{H}}_{\rm mol} = D_M\big(\hat{S}_z^2 - \tfrac{1}{3}S(S+1)\big) + E_M\big(\hat{S}_x^2 - \hat{S}_y^2\big). \quad (5)$$

Spin-orbit interaction can also lead to anisotropy in the exchange Hamiltonian, leading to a general XYZ model whose Hamiltonian is given by

$$\hat{\mathcal{H}}_{\rm XYZ} = \sum_i \sum_j \hat{\vec{s}}_i \cdot \bar{\bar{J}}_{ij} \cdot \hat{\vec{s}}_j, \quad (6)$$

where $\bar{\bar{J}}_{ij}$ is a 3×3 matrix [37]. If the $\bar{\bar{J}}_{ij}$'s are the same for all nearest-neighbor interactions, then by transforming the J matrix to the eigenvector frame of reference results in the XYZ Hamiltonian, which can be written as

$$\hat{\mathcal{H}}_{\rm XYZ} = \sum_{\langle ij \rangle} \big[J^x \hat{s}_i^x \hat{s}_j^x + J^y \hat{s}_i^y \hat{s}_j^y + J^z \hat{s}_i^z \hat{s}_j^z\big]. \quad (7)$$

In this model, there does not exist any spin symmetry and we need to solve the Hamiltonian for its eigenstates in the full Fock basis with no restrictions on total S or M_s. In cases where a system has the same exchange constant along x and y directions but different from the exchange constant in the z direction, we obtain the XXZ model with the Hamiltonian, which is given by

$$\hat{\mathcal{H}}_{\rm XXZ} = \sum_{\langle ij \rangle} J^x \big[\hat{s}_i^x \hat{s}_j^x + \hat{s}_i^y \hat{s}_j^y\big] + J^z \hat{s}_i^z \hat{s}_j^z. \quad (8)$$

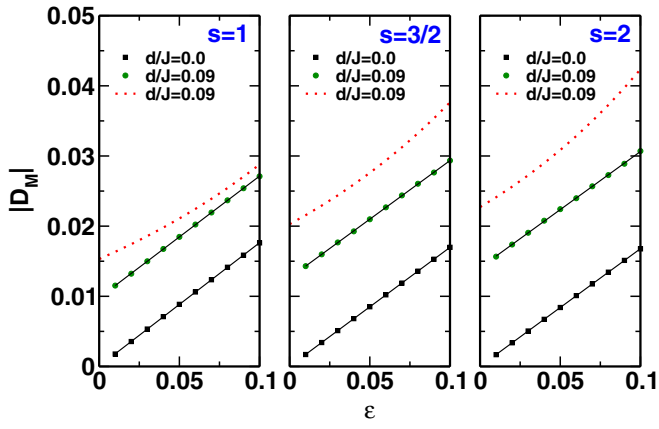

FIG. 1. Dependence of molecular anisotropy parameter $|D_M|$ on ϵ for spin chains with site spins $s = 1$, 3/2, and 2 and chain length $N = 5$. D_M values are computed by fitting the energy gaps to the Hamiltonian $D_M S_z^2$ for on-site anisotropy $d/J = 0$ and 0.09. The error in the fit is largest for $s = 2$ and $d/J = 0.09$ at 4%, which is negligible. The dotted line is from perturbation theory, treating on-site anisotropy as a perturbation, over the eigenstates of the XXZ model.

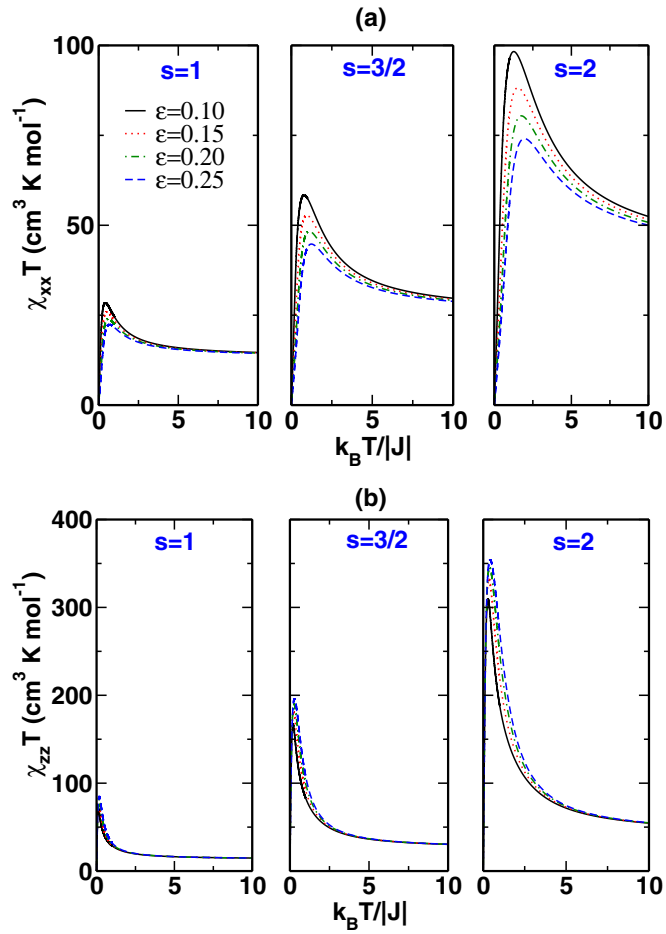

FIG. 2. (a) Plot of $\chi_{xx}T$ as a function of temperature computed with applied field along x direction. (b) Plot of $\chi_{zz}T$ as a function of temperature computed with applied field along z direction for different values of exchange anisotropy ϵ, in the absence of on-site anisotropy. The susceptibilities are computed for field magnitude $H = |J|/g\mu_B = 0.005$. Color coding and line type are the same for all panels. [Note the scales on the y axis are different for (a) and (b)].

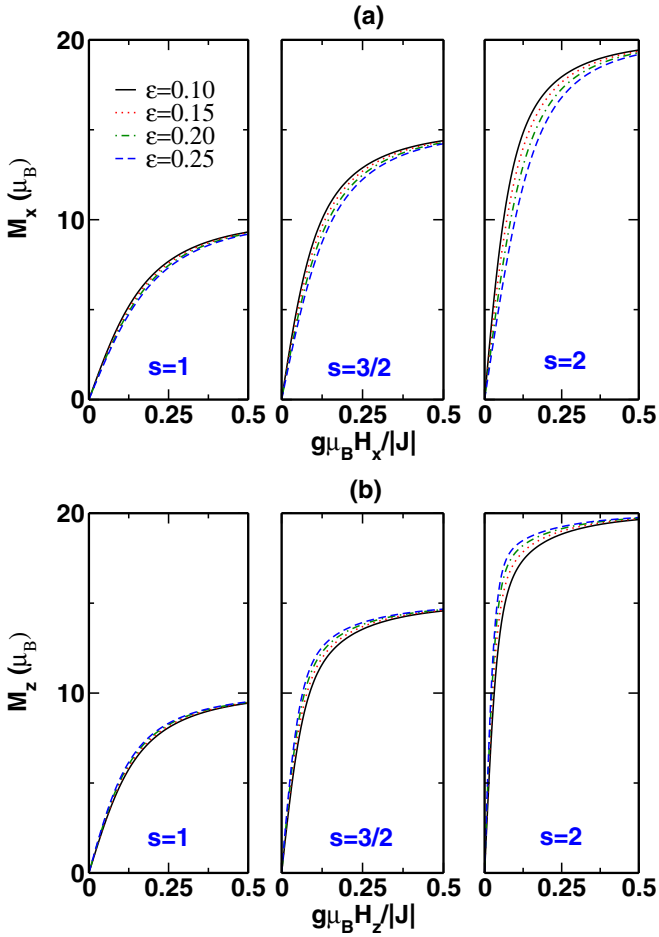

FIG. 3. Dependence of magnetization (M) on applied magnetic field ($g\mu_B H/|J|$) at temperature $k_B T/|J| = 1.0$. (a) M_x versus $g\mu_B H_x/|J|$, (b) M_z versus $g\mu_B H_z/|J|$ for different values of exchange anisotropy ϵ, in the absence of on-site anisotropy. Color coding and line type are the same for all panels.

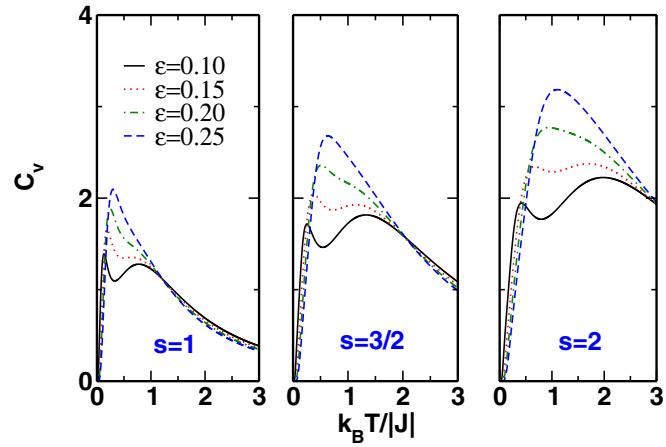

FIG. 4. Dependence of specific heat (C_v) on temperature ($k_B T/|J|$) of spin chains with $s = 1$, $3/2$, and $s = 2$ and systems size $N = 5$ for different values of axial exchange anisotropy ϵ, in the absence of on-site anisotropy. Color coding and line type are the same for all panels.

For convenience, we write the general XYZ Hamiltonian in Eq. (7) as

$$\hat{\mathcal{H}} = \sum_{\langle ij \rangle} J\left[\hat{s}_i^z \hat{s}_j^z + (\gamma + \delta)\hat{s}_i^x \hat{s}_j^x + (\gamma - \delta)\hat{s}_i^y \hat{s}_j^y\right], \qquad (9)$$

where $J^z = J$, $\gamma = \frac{J^x + J^y}{2J}$ and $\delta = \frac{J^x - J^y}{2J}$. The deviation of $\frac{J^x + J^y}{2}$ from J^z is then represented by the parameter $\epsilon = 1 - \gamma$ and the difference between the exchange along x and y directions in normalized units is δ. This model can be solved in the M_s basis. Besides exchange anisotropy, a system can also have site anisotropy, in which case, the $\hat{\mathcal{H}}_{\text{aniso}}$ should be considered together with the respective Hamiltonian, either perturbatively (for weak on-site anisotropy) or in the zeroth-order Hamiltonian itself.

The effect of large anisotropic exchange or large site anisotropy is to mix states with different total spin S. Thus, the conventional approach to define molecular anisotropy constants through the effective Hamiltonian [Eq. (5)] fails as the low-lying multiplet states cannot be identified as arising from a unique total spin state, as the total spin of a state is not conserved. In such situations, the approach we have taken is to obtain the thermodynamic properties such as susceptibility $\chi(T)$, magnetization $M(T)$, and specific heat $C_v(T)$ of the system as a function of Hamiltonian parameters. These are computed from the canonical partition function obtained from the full spectrum of the Hamiltonian. The full Fock space of the Hamiltonian is given by $(2s_i + 1)^N$, where N is the number of sites in the spin chain. The largest system we have studied corresponds to $s_i = 2$ and $N = 5$, which spans a Fock space of dimensionality of 3125. We need to calculate $\langle\langle M_s \rangle\rangle$ for the magnetic properties, which is a thermodynamic average of the expectation values in the eigenstates. To obtain the spin expectation value $\langle \hat{S}^2 \rangle$ in an eigenstate, we have computed the spin-spin correlation functions $\langle \hat{s}_i^z \hat{s}_j^z \rangle$, $\langle \hat{s}_i^x \hat{s}_j^x \rangle$ and $\langle \hat{s}_i^y \hat{s}_j^y \rangle$.

III. ANISOTROPIC EXCHANGE MODELS

Here, we discuss the magnetic anisotropy arising only from the exchange anisotropy. In the small exchange anisotropy limit, we first consider the XXZ model and XYZ model with small δ. We will end this section with a discussion of the XYZ models with large anisotropy parameters ϵ and δ. All the exchange interactions are taken to be ferromagnetic.

A. Small anisotropy XXZ models

In this model, we set δ to zero in Eq. (9) and study spin chains with site spins 1, 3/2, and 2 in chains of four and five sites with open boundary conditions and ferromagnetic exchange interactions. We have not considered spin-1/2 systems since we wish to study the synergistic effect of anisotropic exchange and on-site anisotropy. The latter exists only for site spin greater than half. The ground state in each case corresponds to $\pm M_s = Ns$, where N is the number of sites and s is the site spin. The total spin of the states is calculated from the eigenstates as the expectation value of $\hat{S}^2$.

In Table I, we present the energy gaps from the ground state of the low-lying states up to first $M_s = 0$ state of short

TABLE III. Energy gaps from the ground state (in units of $|J|$) of the low-lying states lying within the manifold of spin $S \simeq ns$ for a five-site spin chain with $s = 1$, 3/2, and 2. Both M_s and S are not conserved and not good quantum numbers. The total spin S_{tot} is calculated from the expectation value $\langle \hat{S}^2 \rangle$ of the state. Intruder states are shown in red. Multiplets beyond the lowest two are shown in green. $\langle M_s \rangle$ are given for states for which it could be computed. $\langle M_s \rangle$ values are not quoted for the states which show large mixing of different M_s states.

$\epsilon = 0.095, \delta = 0.005$								
$s = 1$			$s = 3/2$			$s = 2$		
M_s	S_{tot}	Energy	M_s	S_{tot}	Energy	M_s	S_{tot}	Energy
±5.00	5.00	0	±7.50	7.50	0	±10.00	10.00	0
±4.00	5.00	0.150	±6.50	7.50	0.230	±9.00	10.00	0.301
±3.00	5.00	0.270	±5.50	7.50	0.420	±8.00	10.00	0.570
±1.97	5.00	0.350	±4.50	7.50	0.580	±7.00	10.00	0.810
±1.03	5.00	0.390	±6.50	6.50	0.700	±9.00	9.00	0.932
—	5.00	0.423	±3.50	7.50	0.710	±6.00	10.00	1.015
			±2.43	7.50	0.810	±5.00	9.99	1.190
			±1.51	7.50	0.870	±8.00	9.00	1.195
			±5.50	6.50	0.900	±3.95	10.00	1.332
			—	7.50	0.930	±7.00	9.00	1.430
						—	10.00	1.440
						—	10.00	1.500
						—	10.00	1.540
						—	10.00	1.552
$\epsilon = 0.15, \delta = 0.05$								
±5.00	5.00	0	±7.50	7.50	0	±9.96	10.00	0
±3.80	5.00	0.214	±6.40	7.50	0.330	±8.87	10.00	0.441
—	5.00	0.352	±5.13	7.50	0.610	±7.74	10.00	0.831
—	5.00	0.403	±6.50	6.50	0.800	±8.95	9.00	1.025
—	5.00	0.450	±3.40	7.50	0.820	—	9.98	1.170
±3.93	4.00	0.514	±1.30	7.50	0.981	±7.86	9.00	1.410
—	5.00	0.600	±5.32	6.50	1.040	—	9.98	1.423
			±0.16	7.50	1.200	—	9.98	1.461
			±3.94	6.50	1.253	—	9.98	1.60
			±1.93	6.50	1.410	—	9.98	1.732
			—	7.50	1.480	—	8.98	1.743
			±5.44	5.50	1.533	—	9.98	1.770
			±0.40	6.50	1.565	—	8.97	2.013
			±4.30	5.50	1.740	—	9.98	2.030
			—	6.50	1.790	—	8.98	2.030
			—	7.50	1.820	—	9.98	2.030

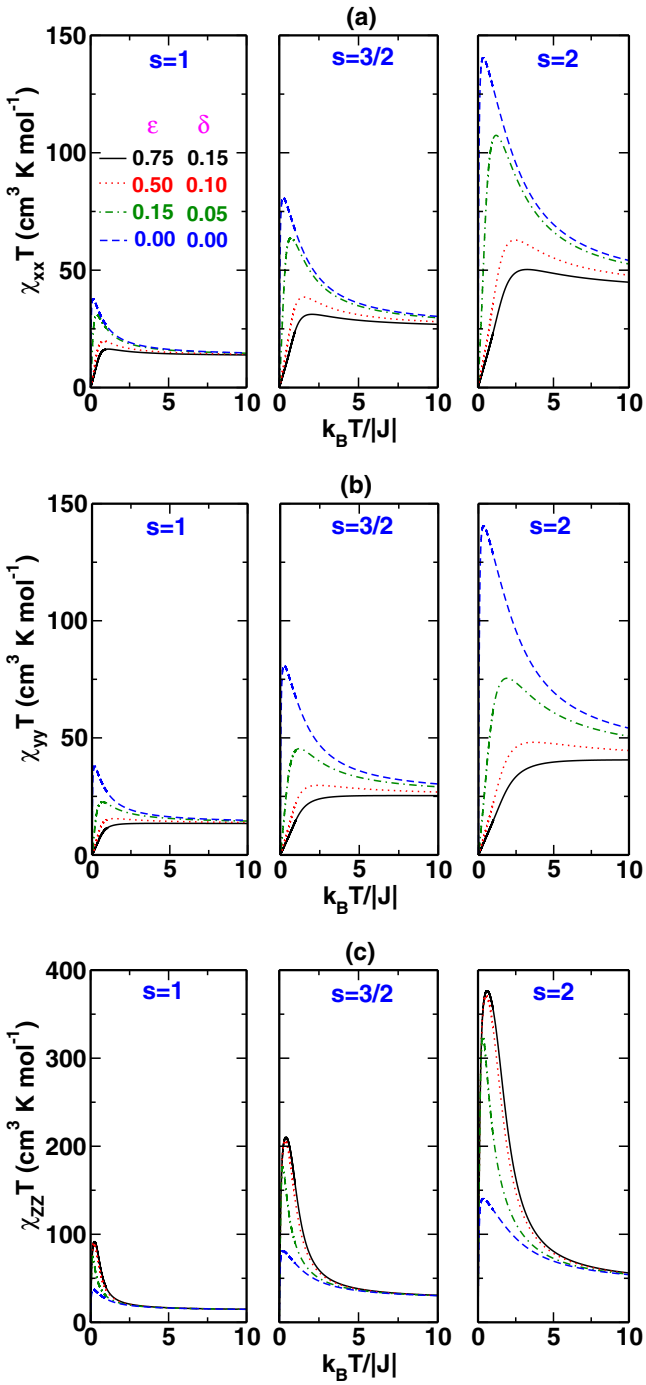

FIG. 5. (a) Plot of $\chi_{xx}T$ as a function of temperature computed with applied field along x direction ($H_x = |J|/g\mu_B = 0.005$), (b) plot of $\chi_{yy}T$ as a function of temperature computed with applied field along y direction ($H_y = |J|/g\mu_B = 0.005$), and (c) plot of $\chi_{zz}T$ as a function of temperature computed with applied field along z direction ($H_z = |J|/g\mu_B = 0.005$) for different values of ϵ and δ, in the absence of on-site anisotropy. Color coding and line type is the same for all panels. [Note scale for (c) is different from those of (a) and (b)].

spin chains of length up to five spins for different ϵ values. The table for spin chains of four spins is given in the Supplemental Material [28]. We notice from the table that for $\epsilon = 0.1$, the lowest energy states of the $s = 1$ chains satisfy $E(|M_s| = Ns) < E(|M_s| = Ns - 1) ... < E(|M_s| = 0)$ and the total spin of these states is also very close to Ns. In this case, we can least-squares fit the energy gaps to the Hamiltonian $D_M S_z^2$ and the error in the fit is negligible. The diagonal anisotropy of these states is shown in Fig. 1. The molecular $|D_M|$ can also be computed by treating d/J as a perturbation and we see that the perturbation theory underestimates $|D_M|$ in all cases and breaks down significantly for large ϵ values and higher site spins. When $d/J = 0$, our perturbation scheme cannot be applied, as it is developed only for systems with anisotropic magnetic centers [27,36]. In the XXZ model, we do not have off-diagonal anisotropy, i.e., $E_M = 0$ in the anisotropic Hamiltonian given by Eq. (5). We note in Table I that for spin

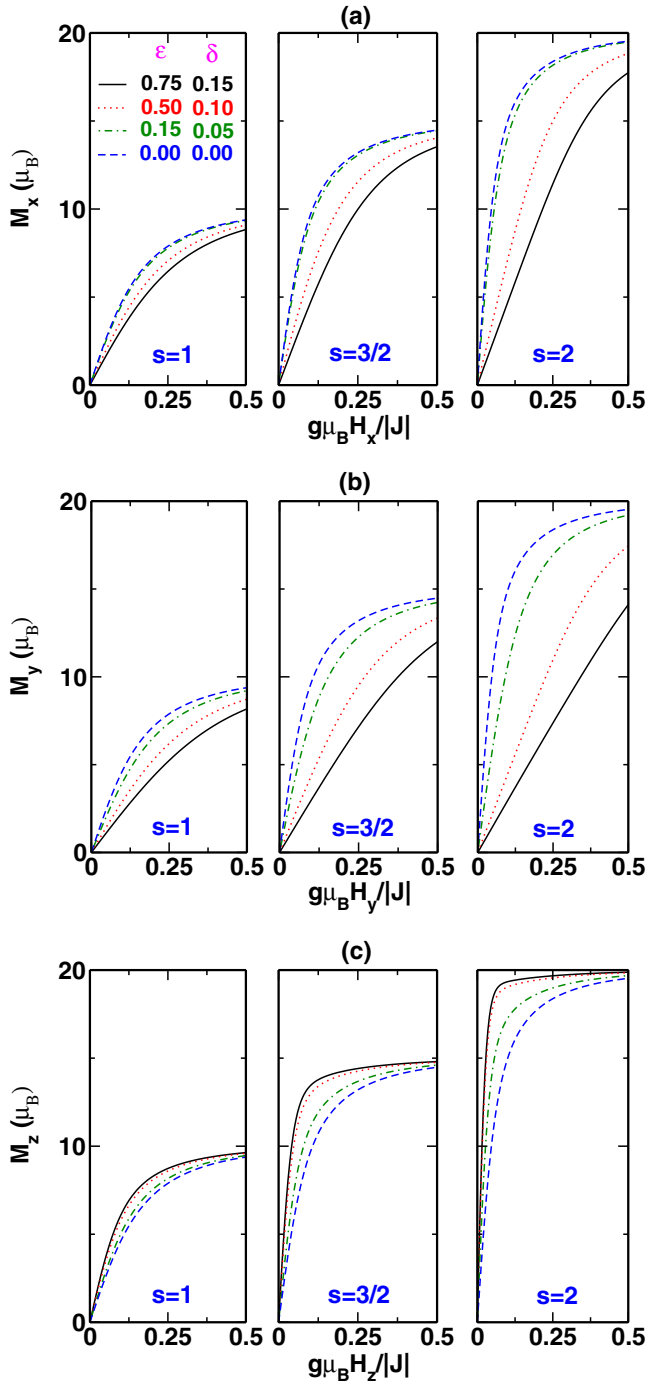

FIG. 6. Dependence of magnetization (M) on applied magnetic field ($g\mu_B H/|J|$) at temperature $k_B T/|J| = 1.0$. (a) M_x versus $g\mu_B H_x/|J|$, (b) M_y versus $g\mu_B H_y/|J|$, and (c) M_z versus $g\mu_B H_z/|J|$ for different values of ϵ and δ, in the absence of on-site anisotropy. Color coding and line type are the same for all panels.

chains with $s = 3/2$ and $s = 2$, there are intruder states within the manifold of $S \simeq 7.5$ and $\simeq 10$, respectively. We also find that as ϵ is increased to 0.15, even the $s = 1$ spin chain has intruders. Furthermore, for site spin 2, the intruders within the $S = 10$ manifold are from progressively lower total spin states, namely $S = 9$, 8, and 7. In this case, however, we are able to fit the spectra of the manifold with approximate spin

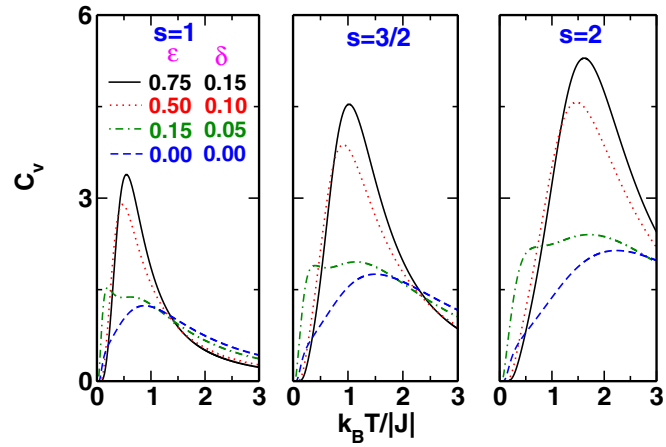

FIG. 7. Dependence of specific heat (C_v) on temperature ($k_B T/|J|$) of spin chains with $s = 1$, $3/2$, and $s = 2$ and systems size $N = 5$ for different values of ϵ and δ, in the absence of on-site anisotropy. Color coding for second and third panels are same as for the first panel.

state (obtained from $\langle \hat{S}^2 \rangle$ of the state) to the Hamiltonian:

$$\hat{\mathcal{H}}_S = E_0(S) + D_M(S)\hat{S}_z^2. \tag{10}$$

We find that the multiplets arising from low-lying total spin states can be described by the above spin Hamiltonian. Values of E_0 and D_M are listed for different total spins for the chain of five $s = 2$ spins in Table II. The D_M values for the low-lying multiplets being close in value may be because the dominant basis states which contribute to the eigenstates of the system are common.

For the $N = 4$ chains, the intruder states occur in the $s = 1$ chain for $\epsilon = 0.25$ and for $s = 3/2$ and $s = 2$ chain for $\epsilon = 0.20$ (see Supplemental Material [28]). Thus, intruders arise at smaller ϵ values for longer chains and higher site spin. The $|D_M|$ increases linearly with increase in anisotropy (Fig. 1).

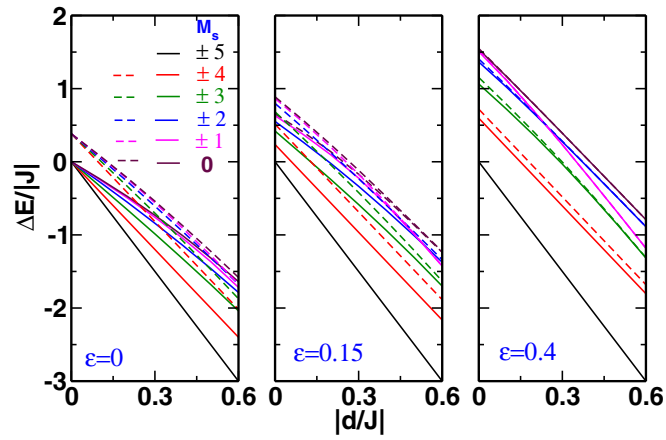

FIG. 8. The effect of on-site anisotropy $|d/J|$ on the splitting of the multiplet states for different strengths of the anisotropy in the XXZ model for the five-site $s = 1$ chain. Solid lines are for the states arising from $S = 5$ state and broken lines are for the states arising from $S = 4$ state. Same color code and line type are used for all panels.

TABLE IV. Energy gaps (in units of $|J|$) from the ground state of the low-lying states lying below the lowest state with $M_s = 0$ for $d/J = 0.1$. M_s is conserved and is a good quantum number. The total spin $S_{\rm tot}$ is calculated from the expectation value of $\langle \hat{S}^2 \rangle$ of the state. Intruder states are shown in red. Multiplets beyond the lowest two are shown in green.

	$N = 5$, d/J = 0.1, XXZ model								
ϵ	$s = 1$			s = 3/2			s = 2		
	M_s	$S_{\rm tot}$	Energy	M_s	$S_{\rm tot}$	Energy	M_s	$S_{\rm tot}$	Energy
0.1	±5	5.00	0	±7.5	7.50	0	±10	10.00	0
	±4	4.99	0.258	±6.5	7.49	0.437	±9	9.99	0.616
	±3	4.98	0.456	±5.5	7.49	0.809	±8	9.99	1.166
	±4	4.00	0.570	±6.5	6.50	0.906	±9	9.00	1.241
	±2	4.97	0.594	±4.5	7.48	1.118	±7	9.98	1.650
	±1	4.95	0.676	±5.5	6.49	1.234	±8	8.99	1.745
	0	4.94	0.703	±3.5	7.46	1.363	±6	9.97	2.067
				±4.5	6.47	1.503	±7	8.98	2.185
				±2.5	7.44	1.545	±5	9.96	2.419
				±1.5	7.45	1.666	±8	8.00	2.427
				±3.5	6.45	1.713	±6	8.96	2.564
				±0.5	7.42	1.726	±4	9.94	2.706
							±7	8.00	2.824
							±5	8.94	2.879
							±3	9.93	2.928
							±2	9.91	3.087
							±4	8.91	3.135
							±6	8.00	3.162
							±1	9.90	3.182
							0	9.90	3.213

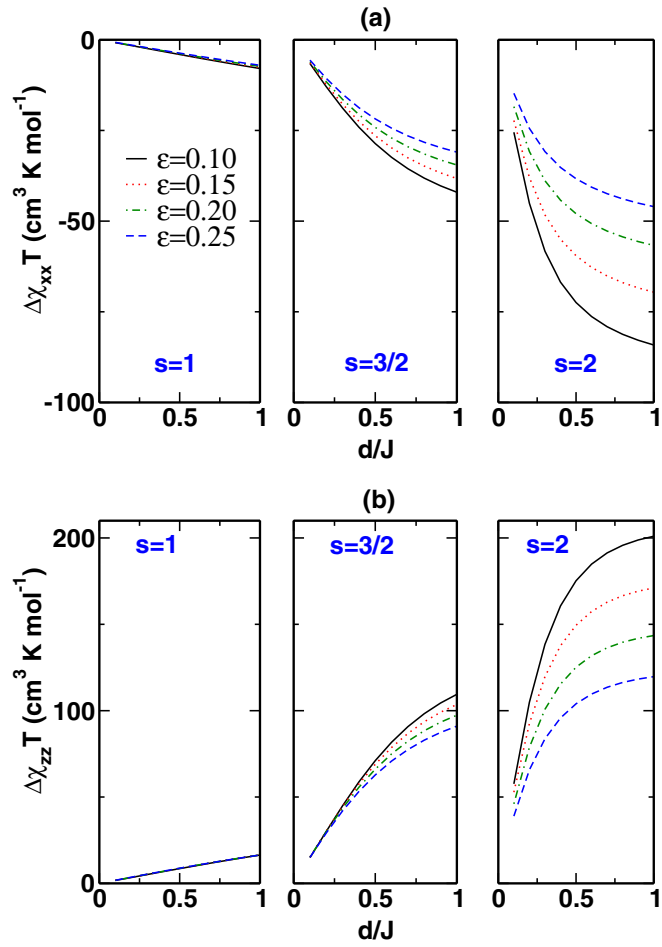

FIG. 9. The effect of on-site anisotropy d/J on (a)$\Delta\chi_{xx}T = [\chi_{xx}T(\epsilon, d \neq 0) - \chi_{xx}T(\epsilon, d = 0)]$ at $g\mu_B H_x/|J| = 0.005$, $k_BT/|J| = 1.0$ and (b) $\Delta\chi_{zz}T = [\chi_{zz}T(\epsilon, d \neq 0) - \chi_{zz}T(\epsilon, d = 0)]$ at $g\mu_B H_z/|J| = 0.005$, $k_BT/|J| = 1.0$ for $\epsilon = 0.10$, 0.15, 0.20 and 0.25. Same color code and line type are used for all panels. Also note the sign of $\Delta\chi_{xx}T$ is –ve while $\Delta\chi_{zz}T$ is +ve.

We have obtained the thermodynamic properties of these spin chains as a function of temperature and the magnetization as a function of magnetic field at a fixed temperature. We show in Fig. 2 $\chi_{xx}T(=\chi_{yy}T)$ and $\chi_{zz}T$ dependence on temperature for spin chains of five spins for different values of the site spins. To obtain the thermodynamic average of the magnetization at a given temperature, we have first calculated the expectation value of the αth component of the magnetization in the eigenstate $|\psi_k\rangle$ as

$$\langle M_k^\alpha \rangle = g\mu_B \langle \psi_k | \hat{S}^\alpha | \psi_k \rangle, \tag{11}$$

where $\hat{S}^\alpha$ ($\alpha = x,\ y,\ z$) are spin operators, g is the gyromagnetic ratio taken as 2, $\beta = \frac{1}{K_BT}$ and μ_B is the Bohr magneton. The thermodynamic average of the expectation values $\langle\langle M^\alpha(T)\rangle\rangle$ are given by

$$\langle\langle M^\alpha(T)\rangle\rangle = \frac{1}{Z}\sum_k e^{-\beta(E_k^0 - g\mu_B H_i \langle M_k^\alpha\rangle)} \langle M_k^\alpha \rangle, \tag{12}$$

where Z is the canonical partition function. The susceptibility $\chi_{\alpha\alpha}$ is then given by $\chi_{\alpha\alpha} = M_\alpha/H_\alpha$ with H_α taken to be $|J|/g\mu_B = 0.005$. Expectedly, the susceptibility increases with site spin in all cases. The $\chi_{zz}T$ component is much larger than the $\chi_{xx}T$ component and both show a maxima. The maxima is at a higher temperature for $\chi_{xx}T$ compared to $\chi_{zz}T$ and the $\chi_{xx}T$ maxima is also broader. We also note that $\chi_{zz}T$ is larger than $\chi_{xx}T$ by a factor of between 2 and 3, even though maximum anisotropy ϵ is only 0.25. Besides, the temperature of the maxima also increases with the increase in site spin. The ZZ component is larger for large anisotropy while the XX component is smaller at large anisotropy. This is because as ϵ increases it becomes easier to magnetize along the z axis, while it becomes harder to magnetize in the x-y plane. This trend is also seen in the magnetization plots as a function of the magnetic field shown in Fig. 3. We note that the magnetization $\langle M_z \rangle$ increases with ϵ while $\langle M_x \rangle$ decreases with ϵ for the same applied field.

The dependence of specific heat, C_v, on temperature for different ϵ values is shown in Fig. 4. We find that for small ϵ, the specific heat shows two peaks, the first peak is narrow and the second peak is broad. This is seen for all site spins. To identify the region of the energy spectrum responsible for the two-peak structure, we calculated specific heat for different energy cutoffs. We found that only for an energy cutoff, $E_{\rm cut} > 3|J|$, the two-peak structure started appearing. Thus, although the second peak occurs around $0.6|J|$, the states contributing to this are at higher energies. Even though the origin of the two-peak structure of the specific heat cannot

be pinpointed, we can still use the magnetic specific heat dependence on temperature as a tool to estimate the anisotropy of the chain.

Introducing small planar anisotropy, δ, does not significantly change the low-energy spectrum in Table III and, consequently, there is no discernible change in the thermodynamic properties. The main difference is that M_s is also not conserved even for small values of δ.

B. Large anisotropy XYZ models

To explore the properties of the spin chains in the large anisotropy limit, we have studied $s = 1$, 3/2, and 2 models with ϵ up to 0.75 and δ up to 0.15. In this limit, there are no conserved spin quantities, hence we have studied only thermodynamic properties by computing thermodynamic averages from expectation values in the eigenstates of the Hamiltonian.

All three diagonal components of the susceptibility as a function of temperature are shown in Fig. 5. We find that for large anisotropy, $\chi_{zz}T$ increases with ϵ and δ, while $\chi_{xx}T$ and $\chi_{yy}T$ decreases with ϵ and δ. $\chi_{zz}T$ shows a smooth maxima for all cases we have studied but $\chi_{xx}T$ and $\chi_{yy}T$ do not show a discernible maxima. The $\chi_{zz}T$ maxima occur at lower temperature than $\chi_{xx}T$ and $\chi_{yy}T$ maxima (when they exist). More significantly, $\chi_{zz}T$ is higher for higher anisotropy while $\chi_{xx}T$ and $\chi_{yy}T$ are higher for lower anisotropy.

In Fig. 6, we show the behavior of magnetization as a function of the field at $k_BT/|J| = 1$. We find very different behavior for M_z compared to M_x or M_y. The M_z component shows saturation at low magnetic fields. The saturation field decreases with increasing site spin. On the other hand, the M_x and M_y components show saturation only for small anisotropy. For large anisotropy, they do not show saturation and show a nearly linear increase in magnetization component over the full range of the applied magnetic field. Furthermore, the magnitude of the magnetization decreases with increasing anisotropy at a given field strength. The specific heat behavior is similar to the weak anisotropy case; we find a sharp peak at low temperature followed by a broad peak at higher temperatures. At higher anisotropies, we find a single peak in the C_v vs T plot 7 and the temperature of the peak maxima is higher for higher anisotropy. For a fixed anisotropy, the peak maximum shifts to higher temperature as the site spin increases from $s = 1$ to $s = 2$.

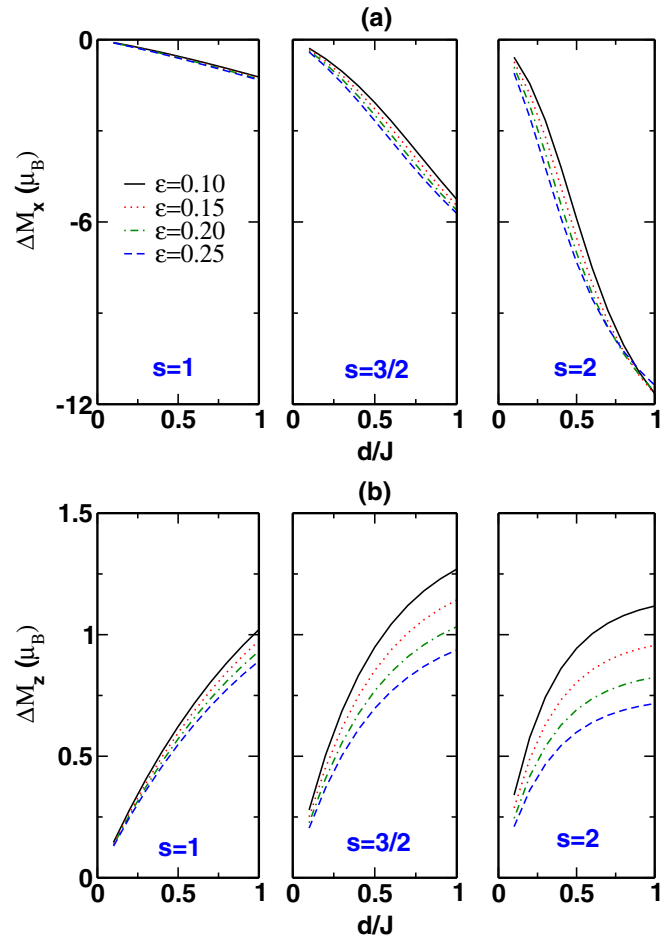

FIG. 10. The effect of on-site anisotropy d/J on (a) $\Delta M_x = M_x(\epsilon, d \neq 0) - M_x(\epsilon, d = 0)$ at $g\mu_B H_x/|J| = 0.25$, $k_BT/|J| = 1.0$, and (b) $\Delta M_z = M_z(\epsilon, d \neq 0) - M_z(\epsilon, d = 0)$ at $g\mu_B H_z/|J| = 0.25$, $k_BT/|J| = 1.0$ for $\epsilon = 0.10$, 0.15, 0.20, and 0.25. Same color and line type are used for all panels.

IV. SYSTEMS WITH XXZ EXCHANGE AND ON-SITE ANISOTROPIES

In an earlier paper, we discussed the role of on-site single ion anisotropy on the anisotropy of a spin chain. In this section we will discuss the effect of both exchange and on-site anisotropy on the magnetic properties of a spin chain [27].

We have introduced on-site anisotropy (d/J) in Eq. (9) and studied the spin chains with site spins $s = 1$, 3/2, and 2 of length of five spins. We have also set $\delta = 0$ and study only XXZ models in the presence of site anisotropy. We have taken the same on-site anisotropy aligned along the z axis for all the spins. When the on-site anisotropy is weak, we find that the resultant molecular magnetic anisotropy is nearly a sum of the molecular anisotropy due to on-site anisotropy alone and the molecular anisotropy due to exchange anisotropy alone. Thus, the two anisotropies are additive, as seen in Fig. 1. This is true up to $\epsilon = 0.1$ for all the site spins.

In Table IV, we show the low-energy spectrum of the $N = 5$ spin chain for $s = 1$, 3/2, and 2, where both exchange and on-site anisotropies are large. In Fig. 8, we show the dependence of the low-lying multiplet energies as a function of the site anisotropy $|d/J|$. We note that as the exchange anisotropy is increased, the multiplets corresponding to different total spins start mixing, and lead to intruder states in the highest spin manifold. In cases where we cannot define the molecular magnetic anisotropy in terms of the parameter D_M of the effective spin Hamiltonian, we follow the system by computing the magnetic susceptibilities, magnetization, and specific heat. We have shown in Fig. 9, the difference in the $\Delta\chi_{xx}T = \chi_{xx}T(\epsilon, d \neq 0) - \chi_{xx}T(\epsilon, d = 0)$ and $\Delta\chi_{zz}T = \chi_{zz}T(\epsilon, d \neq 0) - \chi_{zz}T(\epsilon, d = 0)$ of magnetic susceptibility as a function of d/J at $k_BT/|J| = 1$ for different ϵ values. We find that nonzero d enhances $\Delta\chi_{zz}T$ but decreases $\Delta\chi_{xx}T$ values. In case of site spin $s = 1$, the dependence of $\Delta\chi_{xx}T$ and $\Delta\chi_{zz}T$ on site anisotropy is weak and linear. In case of $s = 3/2$ and $s = 2$, the difference $\Delta\chi_{zz}T$ increases sharply

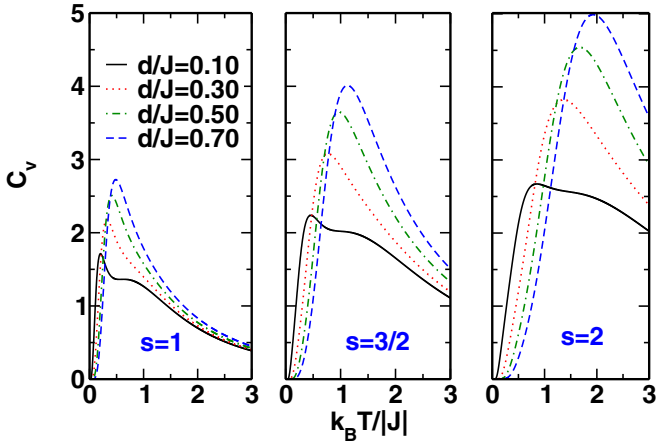

FIG. 11. Dependence of specific heat (C_v) on temperature ($k_BT/|J|$) of spin chains with $s = 1$, 3/2, and $s = 2$ with systems size $N = 5$ for $\epsilon = 0.10$ in the presence of $d/J = 0.10$, 0.30, 0.50, and 0.70. Same color and line type are used for all panels.

as d/J is increased and for higher d/J it tends to saturate. The saturation is more apparent in the $s = 2$ case. $\Delta\chi_{xx}T$ on the other hand decreases with increasing d/J. This is because the on-site anisotropy is oriented along the z axis. This is also the reason why $\Delta\chi_{xx}T$ shows a sharper drop with d/J for larger ϵ while $\Delta\chi_{zz}T$ shows a sharper rise for larger ϵ.

Similarly, in Fig. 10, we plot ΔM_x and ΔM_z for different s and ϵ, as a function of d/J. The field strength is $g\mu_B H = |J|/2$. We note that the ΔM_x decreases sharply with d/J for $s = 2$ and large ϵ while ΔM_z increases with d/J and saturates for $s = 2$ case while in the $s = 3/2$ and $s = 1$ cases, the saturation does not occur even for $d/J = 1.0$. Again ΔM_z is larger when ϵ is small while ΔM_x is larger for large ϵ.

The specific heat behavior is shown in Fig. 11. We find that the two-peak structure persists for small d/J for $\epsilon = 0.1$. However, increasing d/J leads to a single peak. The peak position shifts to higher temperatures as d/J increases and the peak also becomes sharper as d/J increases. This is true for all site spins.

V. CONCLUSIONS

Our study of anisotropic ferromagnetic exchange models with site anisotropy shows that for small exchange and site anisotropies, the energy-level splitting of the total spin states can be characterized by the axial anisotropy parameter D_M, which is a sum of the exchange alone and ion anisotropy alone D_M parameters. For large anisotropic exchange, neither the total spin nor its z component are conserved. However, it is possible to define the molecular anisotropy parameters D_M and E_M for approximate total spin states, with the parameters depending on the total spin. The anisotropy parameters $D_M(S)$ are only weakly dependent on S, and E_M arises for $\delta \neq 0$ and is far smaller than D_M for the parameter range of this study. Since these states will have overlapping multiplets, we have studied the behavior of thermodynamic properties such as χ, C_v, and M. This is also true when the on-site anisotropy is large, even in the absence of exchange anisotropy. We find two-peak structure in C_v vs T when the exchange is weakly anisotropic. We also find that this feature prevails for weak on-site anisotropy as well. The dual peak structure is more pronounced for smaller on-site spins. In general, the effect of anisotropy, as seen from the presence of intruder states from different parent spin states, is more pronounced in the case of higher site spins and longer chain length. The synergy between site anisotropy and exchange anisotropy becomes complicated when both are strong. We observe that the difference in susceptibilities as well as magnetization as a function of the site anisotropy strength for large exchange anisotropy becomes highly nonlinear, particularly for systems with higher site spin.

ACKNOWLEDGMENTS

S.R. and J.-P.S. acknowledge the support through Indo-French Centre for Promotion of Advanced Research (IFCPAR)/Centre Franco-Indien Pour La Promotion de la Recherche Avancee (CEFIPRA) projects. S.R. also thanks Department of Science & Technology for support through different projects and a fellowship and Indian Science Academy for senior scientist position. R.R. thanks Thematic Unit of Excellence-Department of Science & Technology (TUE-DST) for support.

[1] R. Sessoli, D. Gatteschi, H. L. Tsai, D. N. Hendrickson, A. R. Schake, S. Wang, J. B. Vincent, G. Christou, and K. Folting, High-spin molecules:$[Mn_{12}O_{12}(O_2CR)_{16}(H_2O)_4]$, J. Am. Chem. Soc. **115**, 1804 (1993).

[2] R. Sessoli, D. Gatteschi, A. Caneschi, and M. A. Novak, Magnetic bistability in a metal-ion cluster, Nature **365**, 141 (1993).

[3] M. Takahashi, Analytical and numerical investigations of spin chains, Prog. Theor. Phys. **91**, 1 (1994).

[4] J. R. Friedman, M. P. Sarachik, J. Tejada, and R. Ziolo, Macroscopic Measurement of Resonant Magnetization Tunneling in High-Spin Molecules, Phys. Rev. Lett. **76**, 3830 (1996).

[5] L. Thomas, F. Lionti, R. Ballou, D. Gatteschi, R. Sessoli, and B. Barbara, Macroscopic quantum tunneling of magnetization in a single crystal of nanomagnets, Nature **383**, 145 (1996).

[6] G. Christou, D. Gatteschi, D. N. Hendrickson, and R. Sessoli, Single-molecule magnets, MRS Bull. **25**, 66 (2000).

[7] R. Clérac, H. Miyasaka, M. Yamashita, and C. Coulon, Evidence for single-chain magnet behavior in a $Mn^{III} - Ni^{II}$ chain designed with high spin magnetic units: A route to high temperature metastable magnets, J. Am. Chem. Soc. **124**, 12837 (2002).

[8] D. Gatteschi and R. Sessoli, Quantum tunneling of magnetization and related phenomena in molecular materials, Angew. Chem., Int. Ed. **42**, 268 (2003).

[9] C. Coulon, H. Miyasaka, and R. Clérac, Single-chain magnets:Theoretical approach and experimental systems, In *Single-Molecule Magnets and Related Phenomena* (Springer-Verlag, Berlin, 2006).

[10] K. Bernot, L. Bogani, A. Caneschi, D. Gatteschi, and R. Sessoli, A family of rare-earth-based single chain magnets: Playing with anisotropy, J. Am. Chem. Soc. **128**, 7947 (2006).

[11] D. Gatteschi, R. Sessoli, and J. Villain, *Molecular Nanomagnets* (Oxford University Press, Oxford, 2007), p. 316.

[12] S. Demir, M. I. Gonzalez, L. E. Darago, W. J. Evans, and J. R. Long, Giant coercivity and high magnetic blocking temperatures for N_2^{3-} radical-bridged dilanthanide complexes upon ligand dissociation, Nat. Commun. **8**, 2144 (2017).

[13] D. N. Woodruff, R. E. P. Winpenny, and R. A. Layfield, Lanthanide single-molecule magnets, Chem. Rev. **113**, 5110 (2013).

[14] S. K. Langley, D. P. Wielechowski, B. Moubaraki, and K. S. Murray, Enhancing the magnetic blocking temperature and magnetic coercivity of $Cr_2^{III}Ln_2^{III}$single-molecule magnets via bridging ligand modification, Chem. Commun. **52**, 10976 (2016).

[15] R. Ruamps, L. J. Batchelor, R. Maurice, N. Gogoi, P. Jiménez-Lozano, N. Guihéry, C. Degraaf, A. L. Barra, J. P. Sutter, and T. Mallah, Origin of the magnetic anisotropy in heptacoordinate Ni^{II} and Co^{II} complexes, Chem.-Eur. J. **19**, 950 (2013).

[16] N. Gogoi, M. Thlijeni, C. Duhayon, and J. P. Sutter, Heptacoordinated nickel(II) as an Ising-type anisotropic building unit: Illustration with a pentanuclear $[(NiL)_3(W(CN)_8)_2]$ complex, Inorg. Chem. **52**, 2283 (2013).

[17] T. S. Venkatakrishnan, S. Sahoo, N. Bréfuel, C. Duhayon, C. Paulsen, A. L. Barra, S. Ramasesha, and J. P. Sutter, Enhanced ion anisotropy by nonconventional coordination geometry: Single-chain magnet behavior for a $[Fe^{II}L_2Nb^{IV}(CN)_8]$ helical chain compound designed with heptacoordinate Fe^{II}, J. Am. Chem. Soc. **132**, 6047 (2010).

[18] A. K. Bar, C. Pichon, N. Gogoi, C. Duhayon, S. Ramasesha, and J. P. Sutter, Single-ion magnet behavior of heptacoordinated $Fe^{(II)}$ complexes: On the importance of supramolecular organization, Chem. Commun. **51**, 3616 (2015).

[19] A. K. Bar, N. Gogoi, C. Pichon, V. M. L. D. P. Goli, M. Thlijeni, C. Duhayon, N. Suaud, N. Guihíry, A. L. Barra, S. Ramasesha, and J. P. Sutter, Pentagonal bipyramid Fe^{II} complexes: Robust Ising-spin units towards heteropolynuclear nanomagnets, Chem.- Eur. J. **23**, 4380 (2017).

[20] O. Waldmann, A criterion for the anisotropy barrier in single-molecule magnets, Inorg. Chem. **46**, 10035 (2007).

[21] C. J. Milios, A. Vinslava, W. Wernsdorfer, S. Moggach, S. Parsons, S. P. Perlepes, G. Christou, and E. K. Brechin, A record anisotropy barrier for a single-molecule magnet, J. Am. Chem. Soc. **129**, 2754 (2007).

[22] J. Tang, I. Hewitt, N. T. Madhu, G. Chastanet, W. Wernsdorfer, C. E. Anson, C. Benelli, R. Sessoli, and A. K. Powell, Dysprosium triangles showing single-molecule magnet behavior of thermally excited spin states, Angew. Chem., Int. Ed. **45**, 1729 (2006).

[23] J. D. Rinehart and J. R. Long, Exploiting single-ion anisotropy in the design of f-element single-molecule magnets, Chem. Sci. **2**, 2078 (2011).

[24] V. S. Mironov, L. F. Chibotaru, and A. Ceulemans, Mechanism of a strongly anisotropic $Mo^{III}-CN\text{-}Mn^{II}$ spin-spin coupling in molecular magnets based on the $[Mo(CN)_7]^{4-}$ heptacyanometalate: A new strategy for single-molecule magnets with high blocking temperatures, J. Am. Chem. Soc. **125**, 9750 (2003).

[25] M. V. Bennett and J. R. Long, New cyanometalate building units: Synthesis and characterization of $[Re(CN)_7]^{3-}$ and $[Re(CN)_8]^{3-}$, J. Am. Chem. Soc. **125**, 2394 (2003).

[26] R. J. Blagg, L. Ungur, F. Tuna, J. Speak, P. Comar, D. Collison, W. Wernsdorfer, E. J. L. McInnes, L. F. Chibotaru, and R. E. P. Winpenny, Magnetic relaxation pathways in lanthanide single-molecule magnets, Nat. Chem. **5**, 673 (2013).

[27] S. Haldar, R. Raghunathan, J. P. Sutter, and S. Ramasesha, Modelling magnetic anisotropy of single-chain magnets in $|d/J| \geqslant 1$ regime, Mol. Phys. **115**, 2849 (2017).

[28] See Supplemental Material at http://link.aps.org/supplemental/10.1103/PhysRevB.98.214409 for the table corresponding to spin chains of four spins as well as the plots of magnetic susceptibility, specific heat, and magnetization.

[29] S. Carretta, T. Guidi, P. Santini, G. Amoretti, O. Pieper, B. Lake, J. Van Slageren, F. El Hallak, W. Wernsdorfer, H. Mutka, M. Russina, C. J. Milios, and E. K. Brechin, Breakdown of the Giant Spin Model in the Magnetic Relaxation of the Mn6 Nanomagnets, Phys. Rev. Lett. **100**, 157203 (2008).

[30] K. A. Lippert, C. Mukherjee, J. P. Broschinski, Y. Lippert, S. Walleck, A. Stammler, H. Bögge, J. Schnack, and T. Glaser, Suppression of magnetic quantum tunneling in a chiral single-molecule magnet by ferromagnetic interactions, Inorg. Chem. **56**, 15119 (2017).

[31] V. Hoeke, A. Stammler, H. Bögge, J. Schnack, and T. Glaser, Strong and anisotropic superexchange in the single-molecule magnet (SMM) $[Mn_6^{III}Os^{III}]^{3+}$: Promoting SMM behavior through 3d-5d transition metal substitution, Inorg. Chem. **53**, 257 (2014).

[32] J. Dreiser, K. S. Pedersen, A. Schnegg, K. Holldack, J. Nehrkorn, M. Sigrist, P. Tregenna-Piggott, H. Mutka, H. Weihe, V. S. Mironov, J. Bendix, and O. Waldmann, Three-axis anisotropic exchange coupling in the single-molecule magnets $NEt_4[Mn_2^{III}(5-Brsalen)_2(MeOH)_2M^{III}(CN)_6]$ (M = Ru, Os), Chem.- Eur. J. **19**, 3693 (2013).

[33] V. S. Mironov, Origin of dissimilar single-molecule magnet behavior of three $Mn_2^{II}Mo^{III}$ complexes based on $[Mo^{III}(CN)_7]^{4-}$ heptacyanomolybdate: Interplay of $Mo^{III}-CN\text{-}Mn^{II}$ anisotropic exchange interactions, Inorg. Chem. **54**, 11339 (2015).

[34] K. Qian, X.-C. Huang, C. Zhou, X.-Z. You, X.-Y. Wang, and K. R. Dunbar, A single-molecule magnet based on heptacyanomolybdate with the highest energy barrier for a cyanide compound, J. Am. Chem. Soc. **135**, 13302 (2013).

[35] S. Sahoo, R. Rajamani, S. Ramasesha, and D. Sen, Fully symmetrized valence-bond based technique for solving exchange Hamiltonians of molecular magnets, Phys. Rev. B **78**, 054408 (2008).

[36] R. Raghunathan, S. Ramasesha, and D. Sen, Theoretical approach for computing magnetic anisotropy in single molecule magnets, Phys. Rev. B **78**, 104408 (2008).

[37] M. A. Palacios, E. M. Pineda, S. Sanz, R. Inglis, M. B. Pitak, S. J. Coles, M. Evangelisti, H. Nojiri, C. Heesing, E. K. Brechin, J. Schnack, and R. E. P. Winpenny, Copper keplerates: High-symmetry magnetic molecules, Chem. Phys. Chem. **17**, 55 (2016).